




Cite this: *J. Mater. Chem. C*, 2018, 6, 9941

Low temperature and rapid formation of high quality metal oxide thin film *via* a hydroxide-assisted energy conservation strategy†

Meng-Huan Jao, Chien-Chen Cheng, Chun-Fu Lu, Kai-Chi Hsiao and Wei-Fang Su *

Metal oxide thin films made from a sol–gel solution process are promising candidates for stable, low cost, and high performance electronic devices. Reducing the thermal budget required for their crystallization process can relax the fabrication limitation and expand their possible applications. We show that with the addition of an adequate amount of tetramethylammonium hydroxide (TMAOH) in the precursor solution, the activation energy of the sol–gel reaction can be reduced by about 50%. Using this strategy, not only can the required thermal treatment time and temperature of the sol–gel reaction be significantly reduced but also the quality of the film can be improved. The enhanced reaction rate can be ascribed to the presence of hydroxyl anions, which facilitate the formation of the metal hydroxide and the subsequent metal oxide. Additionally, the strategy developed here can be applied to multiple kinds of metal oxides. By this method, the processing temperature can be lowered by at least 50 °C and the time can be shortened by half for the fabrication of electronic devices such as thin film transistors and photovoltaics. Our results open up a new paradigm to fabricate highly crystalline metal oxide thin films quickly at an energy saving low temperature using the solution process.

Received 17th July 2018,
Accepted 21st August 2018

DOI: 10.1039/c8tc03544j

rsc.li/materials-c

Introduction

Nowadays, metal oxide thin films play important roles in modern society, and their potential applications keep expanding, including photovoltaics, thin film transistors (TFTs), sensors, transparent electrodes, electrochromics, *etc.*^{1–4} Many approaches have been developed to prepare high quality metal oxide thin films such as pulse laser deposition, atomic layer deposition, chemical vapor deposition, and radio frequency magnetron sputtering.^{5–8} However, the need for high vacuum conditions, special vapor environments, or expensive equipment raises their production cost and creates obstacles for the process to become commercially feasible. Therefore, a surge of interest has developed for processing metal oxide thin films using a low cost solution approach.

Bearing the advantages ranging from being inexpensive, environmentally friendly, and large area scalable, solution processed metal oxide thin films employ sol–gel chemistry to transform metal–organic precursors into amorphous or

crystalline metal oxides. Typically, these reactions take place at an elevated temperature around 300–400 °C with a time span of tens of minutes. The harsh heat treatment conditions involving a remarkable amount of thermal budget not only limit the choice of substrate, but also increase the complexity of the process and fabrication cost. Understanding and manipulating the chemistry behind the sol–gel reaction provide opportunities to reduce the thermal budget. H. Sirringhaus' group designed and synthesized a metal alkoxide as the precursor.⁹ With the presence of moisture during the annealing process, they found that the hydrolysis reaction for the metal alkoxide can be accelerated, leading to a reduced annealing temperature. T. Marks' group developed a combustion method to realize high performance metal oxide TFTs processed at low temperature.^{10,11} Fuels were added into the precursor solution and ignited during the annealing process, providing extra heat to facilitate the reaction.^{12,13} J. Peng's group recently demonstrated an oxygen radical assisted method to reduce the annealing temperature.¹⁴ By combining the appropriate ratio of nitrate and perchlorate, the release of oxygen radicals can take place at a relatively low temperature of 250 °C and facilitate the reaction. Besides, in order to reduce the thermal budget, energy sources other than heat can be taken into consideration. For example, using photosensitive precursors, light can be another choice to effectively provide energy for the sol–gel crystallization

Department of Materials Science and Engineering and Advanced Research Center for Green Materials Science and Technology, National Taiwan University, Taipei 10617, Taiwan. E-mail: suwf@ntu.edu.tw

† Electronic supplementary information (ESI) available. See DOI: 10.1039/c8tc03544j

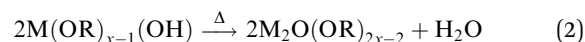
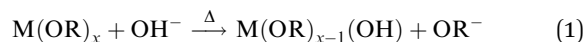
process and fabricate highly crystalline metal oxide thin films at low temperature.¹⁵

Herein, we report the development of a universal approach to efficiently form highly crystalline metal oxide thin films at a temperature reduced by more than 50 °C with an increased reaction rate (*e.g.* reducing the time by half). We manipulate the sol-gel reaction by the addition of organo-ammonium hydroxide salts into the precursor solution. We verify that the presence of hydroxyl anions can induce the efficient formation of the intermediate compound: metal hydroxide, leading to both a reduced time and temperature for the fabrication of crystalline metal oxide thin films. This strategy can be successfully applied to metal oxides including NiO, Co₃O₄, CuO, TiO₂, and In₂O₃. In particular, the performance of metal oxide TFTs and photovoltaics was evaluated and confirmed to be equivalent or superior to that of the conventional metal oxide processed at high temperature. The results demonstrate the potential of our strategy for application to many other metal oxides and their devices.

Results and discussion

Eqn (1) and (2) show typical chemical reactions involved in the formation of a metal oxide in the sol-gel process.¹⁶ The organic part bound to the metal precursor is first protonated and eliminated, followed by the concomitant coordination of the hydroxyl group to the metal ion and the subsequent formation of the metal hydroxide. Under further heat treatment, the M–O–M framework is established, affording crystalline metal oxide thin films. We noticed that for many kinds of metal oxides, the first step of the sol-gel process is the formation of metal hydroxides. Therefore, promoting the reaction rate or tendency of this process may be a promising approach to reduce the thermal budget of solution processed metal oxide thin films. We proposed that, when providing an extra amount of hydroxyl anions, according to Le Chatelier's principle, the system will consume those additional hydroxyl anions by shifting the equilibrium to the right, thereby

enhancing the formation rate of metal hydroxide. The sol-gel NiO thin film system is first studied to examine our hypothesis.



NiO is a potential candidate for p-type transparent semi-conductors, and the protocol of the sol-gel NiO thin film synthesis is currently well-established.^{17–19} Generally, a precursor of nickel, such as nickel acetate, is dissolved in alcohol and stabilized by the coordinating agent ethanolamine. For comparison, we added tetramethylammonium hydroxide (TMAOH) into the NiO precursor solution. We chose TMAOH because of its strong basicity and its ability to provide the hydroxyl anion effectively. In addition, the cation of the organo ammonium can be easily decomposed and removed by heat, remaining as a subtle influence on the final metal oxide thin films. The molar ratios of TMAOH to the nickel precursor were varied from 0 to 0.5, 1.0, and 1.5, and the precursor solutions were named as NiO-T-0, NiO-T-0.5, NiO-T-1.0, and NiO-T-1.5, respectively. Other than NiO-T-1.5, a greenish, homogeneous phase can be obtained for all the precursor solutions. For NiO-T-1.5, the color of the solution was blue, and some undissolved white precipitant was formed. According to ligand field theory, the color of a transition metal ion can be significantly affected by the coordination ligand. Consequently, this indicates a different coordinating condition of the nickel ion when there is 1.5 equivalent of TMAOH.

We fabricated NiO thin films from these precursor solutions by spin-coating. The annealing temperature was set to 250 °C. An obvious change of color from transparent to light grey can be observed after the establishment of the ordered NiO framework. Therefore, judging the change of color can give us a brief idea of reaction rate. A video of annealing NiO thin films with different amounts of TMAOH in the precursor solution was recorded (see ESI†). For the pristine NiO sol-gel solution, NiO-T-0, it took around 12 min to get a greyish film, as it did for NiO-T-0.5. Interestingly, when the concentration of TMAOH

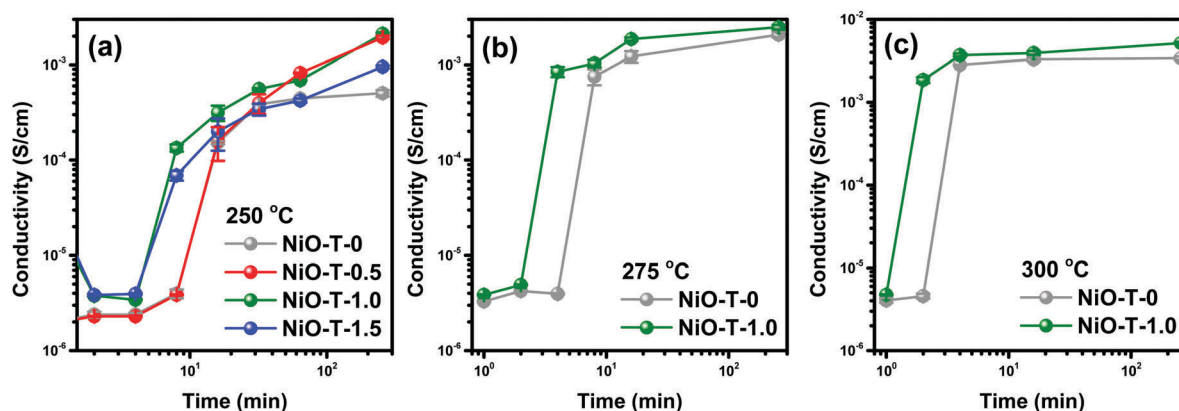


Fig. 1 Conductivity evolution of nickel oxide thin film prepared from sol-gel process. The annealing temperature was set at (a) 250, (b) 275, or (c) 300 °C.

increased, the color change occurred at a much shorter time, 6 min, for the prepared thin film.

Other than the appearance, the conductivity of the NiO thin film can also serve as an indicator to check the formation of crystalline NiO.²⁰ We examined the conductivity of NiO thin film by 4-point probe measurement. Fig. 1(a) illustrates the conductivity of NiO thin films from four different precursor solutions at various annealing times. For both NiO-T-0 (grey line) and NiO-T-0.5 (red line), the conductivity did not reach the order of 10^{-4} S cm^{-1} until 16 min. In contrast, after adding 1.0 (green line) and 1.5 (blue line) equivalent of TMAOH into the precursor solution, it only took around 8 min for the conductivity to achieve the order of 10^{-4} S cm^{-1} . The thin film made from NiO-T-1.5 shows a lower conductivity than NiO-T-1.0. This may be attributed to incomplete decomposition of the tetramethylammonium cation, which deteriorates the overall conductivity. Considering the effectiveness and stability of the precursor solution, we chose a precursor solution containing an equal molar amount of nickel precursor and TMAOH (NiO-T-1.0) for further study.

Similar experiments were carried out at annealing temperatures of 275 and 300 °C. The conductivities of the isothermal samples are summarized in Fig. 1(b) and (c). After the addition of the appropriate amount of TMAOH in the precursor solution, the time required to obtain high conductivity nickel oxide thin film can be reduced by half. One should notice that excellent conductivity can be achieved from TMAOH-assisted NiO thin films after annealing. This could be ascribed to the better film morphology. A more compact and continuous thin film was obtained owing to the presence of organic cation tetramethylammonium as the film-forming agent. The surface roughness (arithmetic mean deviation) of the NiO thin film was lowered from 0.622 to 0.304 nm with the addition of TMAOH (as shown in Fig. S1, ESI†). Therefore, our strategy of adding TMAOH into the NiO precursor solution can both enhance the sol-gel reaction rate and increase the quality of film morphology.

In situ grazing-incidence wide-angle X-ray scattering (GIWAXS) characterization was conducted to investigate the crystallization of NiO thin films during the annealing process.

Fig. 2 compares the time-evolution of diffraction peaks for NiO-T-0 and NiO-T-1.0 when the sol-gel reaction took place at 250 °C. The NiO film adopts the rock salt structure, with diffraction peaks at 37.3° and 43.4° representing (111) and (200), respectively. We assumed the saturation of crystallization was reached when the change of diffraction peak intensity was less than 5%. For the pristine NiO sol-gel thin film, the diffraction peak intensity reached 50% of its saturation value at around 8 min and reached complete saturation at around 32 min. After the addition of TMAOH, the crystallization process seemed to progress much faster. At the initial stage, there were already diffraction peaks indicating the formation of a crystalline NiO structure. The intensity of the diffraction peak quickly reached 50% of its saturation value around 1 min, then fully saturated around 12 min. The diffraction pattern of the TMAOH-assisted NiO thin films exhibited a similar structure to the pristine one. This suggests that the tetramethylammonium cation with highly volatile features can be removed easily. Even in the presence of an equal molar amount of TMAOH as nickel acetate in the NiO-T-1.0 formulation, the crystalline structure was not disturbed by the organic cation. Additionally, these results indicate that the formation of metal hydroxide in the sol-gel process is a rate determining step. Once the transformation of the organic metal precursor into the metal hydroxide occurred, the crystalline metal oxide with a highly ordered structure can be constructed immediately.

We hypothesized that the presence of the hydroxyl anion is critical to the efficient formation of crystalline NiO thin films. Our speculation was verified by a comparable reaction using KOH instead of TMAOH. This time, an equal molar amount of KOH was added into the sol-gel NiO solution and similar experiments were carried out. We noticed that NiO thin films prepared with KOH also turned grey faster than the pristine one, *i.e.*, a shorter time of 6 min rather than the typical time of 12 min at 250 °C. We also measured the conductivity evolution of samples prepared using KOH (Fig. S2, ESI†). However, we would not suggest using KOH as a replacement of TMAOH to increase the sol-gel reaction rate and prepare metal oxide thin films. According to the *in situ* GIWAXS measurement, the

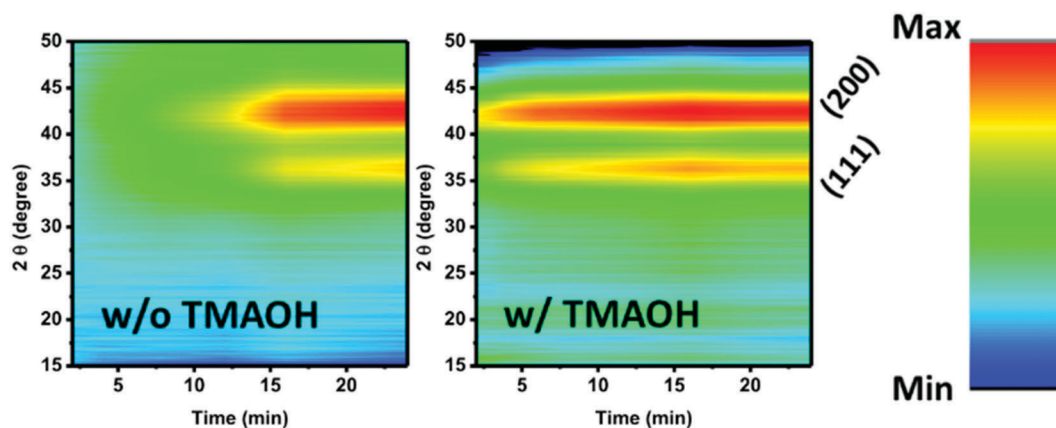


Fig. 2 *In situ* GIWAXS of nickel oxide films prepared by sol-gel process w/o (left) or w/TMAOH (right) annealed at 250 °C.

diffraction peak representing crystalline NiO can be observed at the initial stage, and it reached its saturation value within a short period as well (Fig. S3, ESI†). Nevertheless, different from the TMAOH-assisted sample, the unlikely removal of the potassium cation would ultimately change the material composition and crystalline structure of the as-prepared thin films. This can be asserted by noting the appearance of additional diffraction peaks at 18.9°, 24.7°, and 28.0°.

We also carried out a similar experiment using ammonium hydroxide as a replacement for TMAOH. The result showed that the reaction rate cannot be accelerated by the addition of ammonium hydroxide (Fig. S2, ESI†). One might expect that the same effect could be achieved by adding ammonium hydroxide into the precursor solution. Nevertheless, ammonium hydroxide is formed when ammonia reacts with water molecules in aqueous solution. Ammonia was evaporated off in no time after the thin film deposited from the precursor solution, leading to the disappearance of the respective hydroxyl anion. As a consequence, adding ammonium hydroxide cannot provide the hydroxyl anion during the reaction of the sol-gel process. Based on our investigation, we believe that compounds with a cation that can be readily decomposed upon thermal treatment and an anion providing hydroxide to react with the metal ion can effectively accelerate the crystallization process of NiO thin films.

To unravel the fast formation of the NiO thin film with the assistance of TMAOH, we performed a kinetic study by examining the thin film crystallinity evolution at different temperatures. During the sol-gel reaction under the isothermal condition, the crystallinity *versus* time can be described by the Johnson-Mehl-Avrami (JMA) equation.

$$x(t) = 1 - \exp[-(kt)^n] \quad (3)$$

where x is the crystallinity, k is the rate constant, t is annealing time, and n is the growth exponent. The sol-gel reaction was undertaken at 300, 275, and 250 °C, considering crystallization would reach completion within a reasonable time span. The crystallinity was estimated by the (111) diffraction peaks integrated over all azimuthal angles from GIWAXS measurement (Fig. S4 and S5, ESI†). The rate constant was first determined by fitting experimental data through the JMA equation (Fig. S6, ESI†). The reaction rate here indicates the overall behavior of the formation of metal hydroxide (eqn (1)) and the establishment of the metal oxide framework (eqn (2)). The derived rate constant increases with annealing temperature. We notice that the thin film prepared by NiO-T-1.0 annealed at 250 °C shows a comparable rate constant with the thin film prepared by NiO-T-0 annealed at 300 °C. This can be explained by the rapid increase of (111) diffraction signals in all NiO-T-1.0 thin films. Again, the result supports our speculation that the rate determining step in this reaction is the formation of the metal hydroxide (eqn (1)).

After that, we calculated the activation energy from the rate constant at different temperatures using the Arrhenius equation. For NiO-T-0, the activation energy of the sol-gel reaction is around 107 kJ mol⁻¹ (Fig. S7, ESI†). With the assistance of TMAOH, the activation energy of the sol-gel reaction from NiO-T-1.0 drops significantly to around 59 kJ mol⁻¹. The activation energy we infer here includes the reaction of the organo-metal precursor with the hydroxyl anion to form the metal hydroxide and subsequent condensation of the metal hydroxide into metal oxide. The dramatic reduction of activation energy is a consequence of the existing hydroxyl anion from TMAOH, which alleviates the need for breaking the C-O bond from ethanol or another compound that provides the hydroxyl anion in a typical sol-gel reaction.

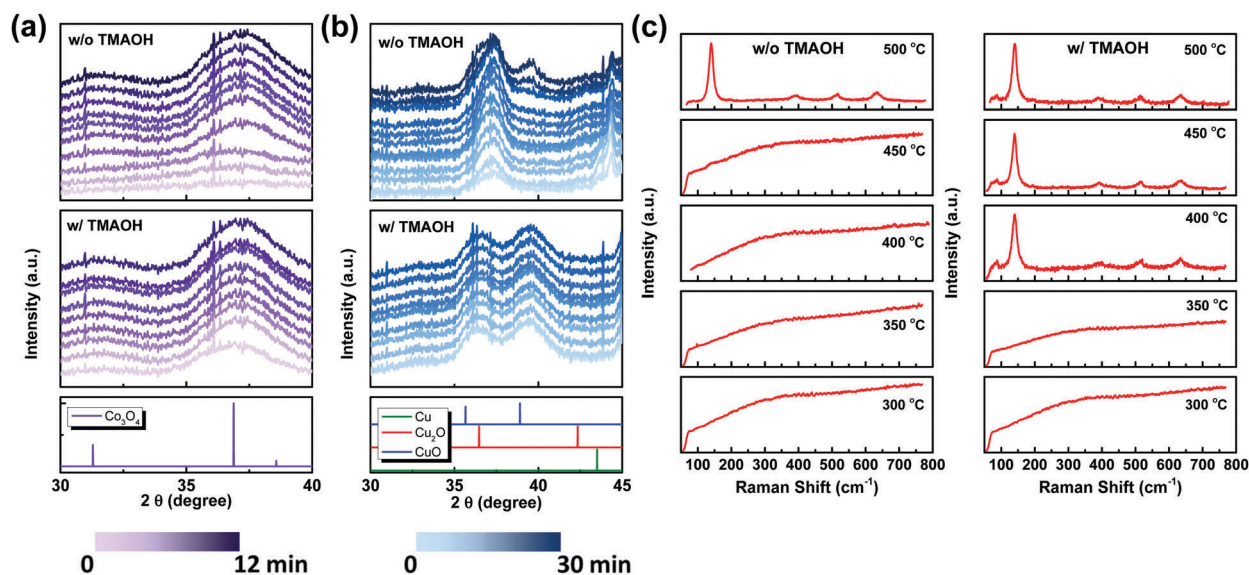


Fig. 3 *In situ* GIWAXS of sol-gel (a) Co₃O₄ and (b) CuO. The top ones are thin films prepared without TMAOH, the bottom ones are thin films with TMAOH. (c) Raman spectra of TiO₂ films prepared by sol gel process. The left part consists of samples prepared without TMAOH, the right part consists of samples prepared with TMAOH. The annealing temperatures from bottom to top are 300, 350, 400, 450, and 500 °C, respectively.

Encouraged by the success of the TMAOH strategy in the NiO system, we applied this approach to other kinds of sol-gel metal oxides such as Co_3O_4 and CuO. The fact that both crystalline Co_3O_4 and CuO appear as greyish or black thin films allows us to roughly estimate the crystallization rate by color. The results showed that, with the addition of TMAOH, the time for color change to take place can be shortened for Co_3O_4 and CuO by half (see ESI†). This fact can be further quantified with the *in situ* GIWAXS study. In Fig. 3(a), the diffraction peak at 36.8° is contributed from $\text{Co}_3\text{O}_4(311)$, which can be used to determine the crystallinity of the Co_3O_4 thin film. For pristine Co_3O_4 without TMAOH, the saturation of crystallinity was reached around 2 min at an annealing temperature of 250°C , while this process can be reduced to less than 1 min in the presence of TMAOH. For CuO, the situation was more complex due to there being two kinds of stable oxide, Cu_2O and CuO. Under thermal annealing at 250°C , the pristine precursor led to Cu_2O at the beginning, and gradually transformed to CuO with prolonged annealing time, as shown in Fig. 3(b). It should be noted that under this annealing condition, a large amount of Cu was produced, as indicated by the diffraction peak at 43.5° . On the other hand, when TMAOH was added into the precursor

solution and then reacted, pure CuO can be formed almost at the beginning of the annealing process without any trace of metal Cu.

Another metal oxide, TiO_2 , was tested to investigate the scope of the TMAOH strategy. Although showing attractive potential in various applications such as photovoltaics, photocatalysts, sensors, *etc.*,^{21–24} the main challenge for TiO_2 is the requirement of a high annealing temperature. Typically, 500°C is used to obtain highly crystalline anatase TiO_2 thin films. Therefore, we fabricated TiO_2 thin films with different annealing temperatures from 300 to 500°C and examined whether the TMAOH strategy can reduce the annealing temperature. Fig. 3(c) shows the Raman spectra of a TiO_2 thin film on Au/Si fabricated at different annealing temperatures. For the pristine solution, the signals representing the anatase phase of TiO_2 can only be detected when the annealing temperature reaches 500°C . Significantly, the addition of TMAOH can successfully lower the required temperature. The appearance of the anatase phase of TiO_2 can be clearly observed in the Raman spectrum at an annealing temperature as low as 400°C .

We took a further step to fabricate metal oxide electronic devices using the TMAOH strategy. This time, another metal

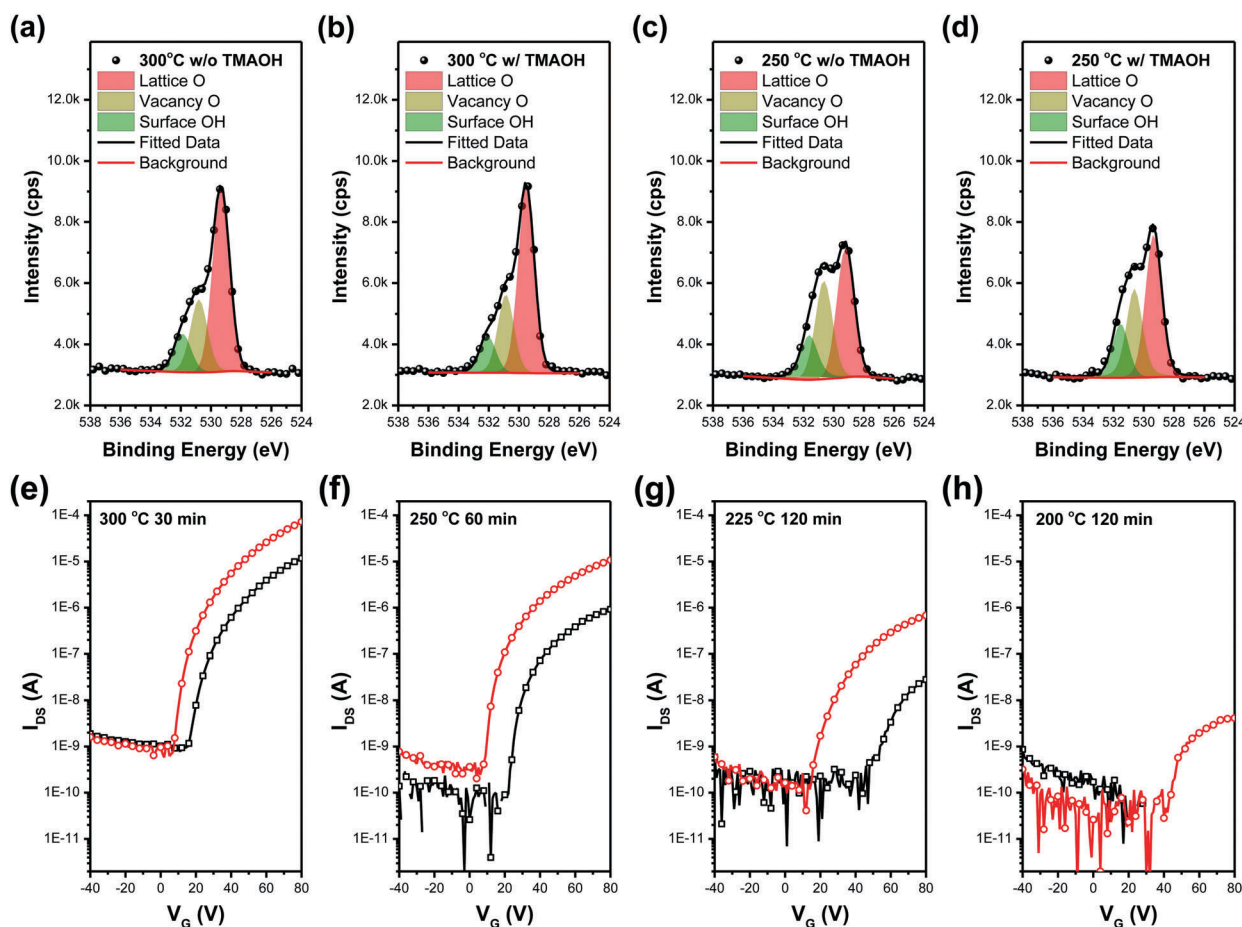


Fig. 4 XPS spectra of O 1s from In_2O_3 thin film. The fabrication conditions were (a) 300°C w/o TMAOH, (b) 300°C w/TMAOH, (c) 250°C w/o TMAOH, or (d) 250°C w/ TMAOH. Transfer characteristics of In_2O_3 TFT. Black lines were devices made w/o TMAOH, red lines were devices made w/TMAOH. The fabrication conditions were (e) 300°C for 30 min, (f) 250°C for 60 min, (g) 225°C for 120 min, and (h) 200°C for 120 min.

oxide, In_2O_3 , was tested. Solution processed In_2O_3 is widely studied and used as the channel material for TFTs.^{25–27} Thin films made from both pristine and TMAOH-assisted precursor solutions were annealed at different temperatures. Fig. 4(a)–(d) and Table S1 (ESI[†]) summarize the results of X-ray photoelectron spectroscopy (XPS) characterization of the as-prepared thin films. The XPS technique can distinguish elements having different chemical environments or oxidation states. In terms of oxygen, signals coming from lattice oxygen, vacancy oxygen, and surface hydroxyl oxygen can be unambiguously determined. When the annealing temperature was set at 300 °C, the ratios of lattice oxide to vacancy oxide seem to show little difference between samples prepared from the pristine solution or the TMAOH-assisted solution. However, when the annealing temperature decreased, say at 250 °C, the effect of TMAOH became pronounced, forming a greater amount of lattice oxide than that of the pristine one. In addition to XPS analysis, the GIWAXS measurement (Fig. S8, ESI[†]) also provides consistent results. The (222) and (400) diffraction peaks of cubic phase In_2O_3 can only be detected for a sample fabricated at 300 °C from the pristine solution, while noticeable diffraction peaks can be observed even for a sample fabricated at 225 °C from the precursor solution containing TMAOH.

Bottom gate top contact In_2O_3 TFTs were made, with Si as the bottom gate, SiO_2 as the dielectric, and thermally deposited Al as the top contact. The transfer characteristics of In_2O_3 TFTs are shown in Fig. 4(e)–(h). The annealing temperature of In_2O_3 was varied from 200 to 300 °C. It was found that, at every

annealing temperature, devices made from the TMAOH-assisted solution always outperform the devices made from the pristine solution, which can be explained by the XPS and GIWAXS characterization that rapid and efficient formation of crystalline In_2O_3 can be achieved from the TMAOH-assisted solution. Furthermore, when the annealing temperature was decreased to 200 °C, pristine In_2O_3 exhibited no further transistor behavior. In comparison, the device made from the TMAOH added solution can still be turned on at a gate voltage of 40 V.

In order to demonstrate the efficient formation of crystalline metal oxide thin films without sacrificing electronic or interfacial integrity, organic–inorganic hybrid perovskite (OIHP) photovoltaics based on NiO as the hole transport layer were fabricated.^{28,29} The morphology of solution processed OIHP thin films is sensitive to the substrate, and the interfaces between OIHP and the charge carrier transport layer are responsible for the efficient carrier extraction process.^{30–32} Both conditions are required to obtain high performance OIHP devices. Therefore, we expected that fabricating OIHP photovoltaics based on TMAOH-assisted NiO thin films would be a convincing approach to verify the bulk and interface properties of the as-made thin films.

Fig. 5, and Tables S2, S3 (ESI[†]) illustrate the I - V characterization curves and some key parameters of OIHP photovoltaics based on NiO thin films. To be an applicable hole transport layer, criteria of good conductivity and the appropriate energy level are critical and need to be fulfilled at the same time. In the literature, the typical annealing condition for NiO thin films is

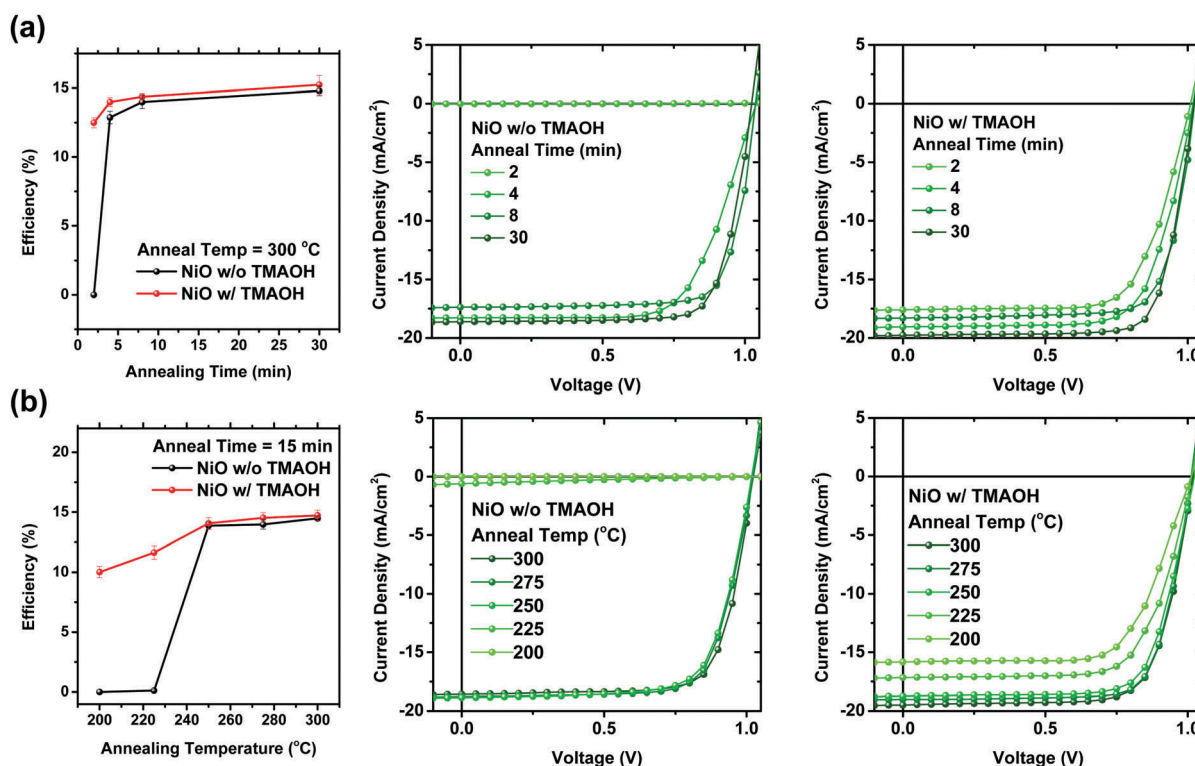


Fig. 5 The performance of OIHP photovoltaics based on NiO thin films. (a) Summary and I - V characterization curves of device efficiencies with various NiO annealing times at 300 °C. (b) Summary and I - V characterization curves of device efficiencies with various NiO annealing temperatures.

300 °C for 30 min.^{33,34} In our experiments, we fixed the annealing temperature to be 300 °C, and different annealing times were examined. For the pristine NiO solution, the perovskite device exhibits no photodiode characteristics nor noticeable efficiency when the annealing time of the NiO thin film is shorter than 4 min. Thus, a NiO thin film with an annealing time of more than 4 min is required to function as an appropriate hole transport layer in a high performance perovskite device. On the other hand, the TMAOH strategy can greatly increase the reaction rate of the NiO sol-gel process, and an annealing time of 2 min is enough to obtain high performance perovskite devices. The results are summarized in Fig. 5(a) and Table S2 (ESI[†]). Importantly, the efficiency of the perovskite photovoltaics can be significantly affected by the interface between perovskite thin films and carrier transporting layers. The devices based on TMAOH-assisted NiO thin films exhibited comparable or even higher efficiencies than the pristine one, suggesting either that the ammonium cations can be completely removed from the thin film during thermal treatment or that the remaining ammonium cations would not deteriorate the perovskite crystalline structure. This again demonstrates the efficient formation of crystalline NiO by the TMAOH strategy. Therefore, using this approach, the thermal budget of the NiO sol-gel process can be significantly reduced.

Motivated by our results, we further explored the minimum annealing temperature required to achieve suitable NiO thin films for perovskite devices. This time, the annealing time was set to be 15 min, and various annealing temperatures were tested ranging from 200 to 300 °C. The results are shown in Fig. 5(b) and Table S3 (ESI[†]). An annealing temperature higher than 250 °C is required using pristine NiO thin films. Once the processing temperature is reduced to 225 °C, there is no crystalline NiO produced, leading to poor device performance. Using the TMAOH strategy, we noticed that crystalline NiO can be produced at a temperature as low as 200 °C in a short period (15 min), and perovskite devices with an efficiency of 10% can be obtained. Therefore, we demonstrated that the TMAOH-assisted strategy can successfully reduce the thermal budget while producing high quality NiO thin films applicable for perovskite photovoltaics.

Conclusions

We develop a promising energy saving method to reduce both the time and temperature required to fabricate highly crystalline metal oxide thin films. We provide hydroxyl anions and manipulate the typical sol-gel reaction by adding TMAOH into the metal oxide precursor and obtain a homogeneous and stable solution. Careful investigation reveals that during the thermal treatment process, the hydroxyl anion released from TMAOH can accelerate the formation of the metal hydroxide, leading to an increased overall reaction rate and reduced activation energy. Because the reaction shows no specific requirement in the selection of metal ions, this method can be generalized to many other kinds of metal oxide systems,

such as NiO, Co₃O₄, CuO, TiO₂ and In₂O₃, as demonstrated in this study. The performance of electronic devices using the TMAOH-assisted strategy is also examined. For In₂O₃ TFTs, a higher turn-on current can be extracted, and the transistor behavior can be observed at a lower processing temperature. For NiO based OIHP photovoltaics, a shorter annealing time and lower annealing temperature can be used to obtain the crystalline NiO thin film for high efficiency OIHP photovoltaics. Therefore, this approach is a promising strategy to reduce the thermal budget for various sol-gel metal oxide thin films and is applicable to the synthesis of high performance metal oxide based electronic devices.

Experimental

Chemicals

NiO pristine sol-gel solution was prepared by dissolving nickel acetate tetrahydrate in ethanol at 60 °C to obtain 1 M (for conductivity measurement and GIWAXS analysis) or 0.5 M (for photovoltaic application) green solutions, followed by dropping an equal molar amount of ethanolamine as stabilizer. Co₃O₄ pristine sol-gel solution was prepared by dissolving 0.5 M cobalt acetate in ethanol/water (v/v = 1/1) with equal molar ethanolamine to obtain a dark purple solution. Copper acetate was dissolved in ethanol to obtain a 0.5 M dark blue solution with 1 M ethanolamine as stabilizer. Titanium diisopropoxide bis(acetylacetonate) was dispersed in ethanol to obtain a 0.5 M pale yellow solution with 0.5 M ethanolamine as stabilizer. To prepare the In₂O₃ precursor solution, 1 mmol of indium acetate was dissolved in 10 mL of 2-methoxyethanol with the aid of 2 mmol of ethanolamine and 0.4 mL of ammonium solution (28.0–30.0%).

For the TMAOH-assisted precursor solution, to obtain a stable and homogeneous solution, the molar concentration of TMAOH was equal to the metal salt while keeping all the other formulations unchanged. For example, the NiO precursor solution for photovoltaic application was prepared by dissolving 0.5 M nickel acetate tetrahydrate, 0.5 M ethanolamine, and 0.5 M TMAOH in ethanol.

Metal oxide thin film preparation

For simplicity, in our experiments, all the metal oxide thin films were prepared by spin-coating the respective metal oxide precursor solutions on substrates at 4000 rpm for 20 s. Glass, Si wafer, or Si/Au was selected as the substrate when preparing samples for 4-point probe measurement, GIWAXS analysis, or Raman characterization, respectively. A hotplate containing a feedback control system was used to anneal the sol-gel metal oxide thin films. The temperature of the hotplate was first stabilized at the desired condition before placing samples on the preheated hotplate.

Metal oxide thin film characterization

Four-point probe measurement was conducted on a commercial probe station (Solar Energy Tech, FPSR100a), data were recorded

and analyzed by the LabView program. Synchrotron GIWAXS measurement was performed at the end station BL23A1 of the National Synchrotron Radiation Research Center (NSRRC), Taiwan.³⁵ Monochromated X-rays of 10 and 15 keV were used as the light source. The incident angle was kept at 1°. For *in situ* measurement, a custom-built heater was used as a sample stage. The Raman spectrum (WITec, Alpha300 S) with a 632.8 nm He–Ne laser was recorded on a high-resolution piezoelectric stage of a scanning microscope. The XPS data were collected from a PHI 5000 VersaProbe (ULVAC-PHI, Chigasaki, Japan) system with a microfocused (100 mm, 25 W) Al X-ray beam. During the measurement, the pressure of the main chamber was kept below 10⁻⁷ Pa by means of turbomolecular and ion-getter pumps.

In₂O₃ TFT fabrication and characterization

Highly p-doped Si wafer with 300 nm thick thermal oxide was used as the substrate, which was cleaned by subsequent sonication in acetone, methanol, and isopropanol, then a 15 min oxygen plasma treatment was used just prior to spin coating. A thin layer of In₂O₃ was deposited on the Si wafer by spin coating In₂O₃ precursor solution at 4000 rpm for 20 s. After thermal treatment, 100 nm thick Al was immediately thermally deposited as the source and drain through a shadow mask. The channel length (*W*) and width (*L*) are 1000 μm and 100 μm, respectively. TFT characterization was carried out by a Keysight B2912A precision source/measure unit.

NiO-based perovskite photovoltaic fabrication and characterization

The NiO precursor solution was spin-coated on pre-cleaned FTO at 4000 rpm for 20 s, followed by the designed annealing process. Typically, it takes 30 min at 300 °C for complete crystallization. In our work, we also tested a shorter annealing time and a lower annealing temperature. The OIHP thin film was spin coated from the precursor solution of methylammonium iodide (1 M) and lead iodide (1 M) in DMF/DMSO (*v/v* = 5/2). After 16 s spin coating at 4500 rpm, 300 μL of diethyl ether was dropped on the OIHP thin film to wash out excess solvent. A compact OIHP thin film can be obtained after thermal treatment of 1 min at 75 °C and 2 min at 100 °C. The electron transport layer of PCBM (20 mg mL⁻¹ in chlorobenzene) and PEI (0.1 wt% in isopropanol) were spin-coated at 1000 rpm and 3000 rpm, respectively. Finally, 100 nm of Ag was thermally deposited as the top electrode. The photovoltaic characterization was performed by using a Keithley 2410 source meter, with the device under AM1.5G illumination (100 mW cm⁻²).

Conflicts of interest

The authors declare no conflicts of interest.

Acknowledgements

The authors thank the Ministry of Science and Technology of Taiwan for financial support for this research (106-3113-E-002-008-CC2,

106-2119-M-002-030). This work was also financially supported by the “Advanced Research Center for Green Materials Science and Technology” from The Featured Area Research Center Program within the framework of the Higher Education Sprout Project by the Ministry of Education (107L9006) and the Ministry of Science and Technology in Taiwan (MOST 107-3017-F-002-001).

References

- 1 X. Yu, T. J. Marks and A. Facchetti, *Nat. Mater.*, 2016, **15**, 383–396.
- 2 M. K. Brennaman, R. J. Dillon, L. Alibabaei, M. K. Gish, C. J. Dares, D. L. Ashford, R. L. House, G. J. Meyer, J. M. Papanikolas and T. J. Meyer, *J. Am. Chem. Soc.*, 2016, **138**, 13085–13102.
- 3 Z. Wang, P. K. Nayak, J. A. Caraveo-Frescas and H. N. Alshareef, *Adv. Mater.*, 2016, **28**, 3831–3892.
- 4 W. C. Choy and D. Zhang, *Small*, 2016, **12**, 416–431.
- 5 L.-X. Qian, Z.-H. Wu, Y.-Y. Zhang, P. T. Lai, X.-Z. Liu and Y.-R. Li, *ACS Photonics*, 2017, **4**, 2203–2211.
- 6 H. Van Bui, F. Grillo and J. R. van Ommen, *Chem. Commun.*, 2017, **53**, 45–71.
- 7 D. Barreca, G. Carraro, A. Gasparotto, C. Maccato, T. Altantzis, C. Sada, K. Kaunisto, T.-P. Ruoko and S. Bals, *Adv. Mater. Interfaces*, 2017, **4**, 1700161.
- 8 L. Petti, N. Münzenrieder, C. Vogt, H. Faber, L. Büthe, G. Cantarella, F. Bottacchi, T. D. Anthopoulos and G. Tröster, *Appl. Phys. Rev.*, 2016, **3**, 021303.
- 9 K. K. Banger, Y. Yamashita, K. Mori, R. L. Peterson, T. Leedham, J. Rickard and H. Sirringhaus, *Nat. Mater.*, 2011, **10**, 45–50.
- 10 M. G. Kim, M. G. Kanatzidis, A. Facchetti and T. J. Marks, *Nat. Mater.*, 2011, **10**, 382–388.
- 11 B. Wang, L. Zeng, W. Huang, F. S. Melkonyan, W. C. Sheets, L. Chi, M. J. Bedzyk, T. J. Marks and A. Facchetti, *J. Am. Chem. Soc.*, 2016, **138**, 7067–7074.
- 12 J. W. Jung, C. C. Chueh and A. K. Jen, *Adv. Mater.*, 2015, **27**, 7874–7880.
- 13 A. Varma, A. S. Mukasyan, A. S. Rogachev and K. V. Manukyan, *Chem. Rev.*, 2016, **116**, 14493–14586.
- 14 P. Gao, L. Lan, Z. Lin, S. Sun, Y. Li, W. Song, E. Song, P. Zhang and J. Peng, *Chem. Commun.*, 2017, **53**, 6436–6439.
- 15 I. Bretos, R. Jiménez, J. Ricote and M. L. Calzada, *Chem. Soc. Rev.*, 2018, **47**, 291–308.
- 16 C. J. Brinker and G. W. Scherer, *Sol-gel science: the physics and chemistry of sol-gel processing*, Academic Press, Boston, 1990.
- 17 J. R. Manders, S.-W. Tsang, M. J. Hartel, T.-H. Lai, S. Chen, C. M. Amb, J. R. Reynolds and F. So, *Adv. Funct. Mater.*, 2013, **23**, 2993–3001.
- 18 Q. Liu, Q. Chen, Q. Zhang, Y. Xiao, X. Zhong, G. Dong, M.-P. Delplancke-Ogletree, H. Terryn, K. Baert, F. Reniers and X. Diao, *J. Mater. Chem. C*, 2018, **6**, 646–653.
- 19 J. You, L. Meng, T. B. Song, T. F. Guo, Y. M. Yang, W. H. Chang, Z. Hong, H. Chen, H. Zhou, Q. Chen, Y. Liu, N. De Marco and Y. Yang, *Nat. Nanotechnol.*, 2016, **11**, 75–81.

- 20 A. Liu, H. Zhu, Z. Guo, Y. Meng, G. Liu, E. Fortunato, R. Martins and F. Shan, *Adv. Mater.*, 2017, **29**, 1701599.
- 21 M.-C. Wu, H.-H. Lo, H.-C. Liao, S. Chen, Y.-Y. Lin, W.-C. Yen, T.-W. Zeng, Y.-F. Chen, C.-W. Chen and W.-F. Su, *Sol. Energy Mater. Sol. Cells*, 2009, **93**, 869–873.
- 22 M.-C. Wu, J. Hiltunen, A. Sápi, A. Avila, W. Larsson, H.-C. Liao, M. Huuhtanen, G. Tóth, A. Shchukarev, N. Laufer, Á. Kukovecz, Z. Kónya, J.-P. Mikkola, R. Keiski, W.-F. Su, Y.-F. Chen, H. Jantunen, P. M. Ajayan, R. Vajtai and K. Kordás, *ACS Nano*, 2011, **5**, 5025–5030.
- 23 J. Bai and B. Zhou, *Chem. Rev.*, 2014, **114**, 10131–10176.
- 24 L. Tian, J. Xu, M. Just, M. Green, L. Liu and X. Chen, *J. Mater. Chem. C*, 2017, **5**, 4645–4653.
- 25 H. S. Kim, M.-G. Kim, Y.-G. Ha, M. G. Kanatzidis, T. J. Marks and A. Facchetti, *J. Am. Chem. Soc.*, 2009, **131**, 10826–10827.
- 26 I. Isakov, H. Faber, M. Grell, G. Wyatt-Moon, N. Pliatsikas, T. Kehagias, G. P. Dimitrakopoulos, P. P. Patsalas, R. Li and T. D. Anthopoulos, *Adv. Funct. Mater.*, 2017, **27**, 1606407.
- 27 J. Leppaniemi, O. H. Huttunen, H. Majumdar and A. Alatalo, *Adv. Mater.*, 2015, **27**, 7168–7175.
- 28 Z. H. Bakr, Q. Wali, A. Fakhruddin, L. Schmidt-Mende, T. M. Brown and R. Jose, *Nano Energy*, 2017, **34**, 271–305.
- 29 S. Yue, K. Liu, R. Xu, M. Li, M. Azam, K. Ren, J. Liu, Y. Sun, Z. Wang, D. Cao, X. Yan, S. Qu, Y. Lei and Z. Wang, *Energy Environ. Sci.*, 2017, **10**, 2570–2578.
- 30 Y. Bai, H. Chen, S. Xiao, Q. Xue, T. Zhang, Z. Zhu, Q. Li, C. Hu, Y. Yang, Z. Hu, F. Huang, K. S. Wong, H.-L. Yip and S. Yang, *Adv. Funct. Mater.*, 2016, **26**, 2950–2958.
- 31 C. Bi, Q. Wang, Y. Shao, Y. Yuan, Z. Xiao and J. Huang, *Nat. Commun.*, 2015, **6**, 7747.
- 32 M. Cha, P. Da, J. Wang, W. Wang, Z. Chen, F. Xiu, G. Zheng and Z.-S. Wang, *J. Am. Chem. Soc.*, 2016, **138**, 8581–8587.
- 33 W. Chen, Y. Wu, Y. Yue, J. Liu, W. Zhang, X. Yang, H. Chen, E. Bi, I. Ashraful, M. Grätzel and L. Han, *Science*, 2015, **350**, 944–948.
- 34 H.-C. Liao, P. Guo, C.-P. Hsu, M. Lin, B. Wang, L. Zeng, W. Huang, C. M. M. Soe, W.-F. Su, M. J. Bedzyk, M. R. Wasielewski, A. Facchetti, R. P. H. Chang, M. G. Kanatzidis and T. J. Marks, *Adv. Energy Mater.*, 2017, **7**, 1601660.
- 35 C.-Y. Chang, Y.-C. Huang, C.-S. Tsao and W.-F. Su, *ACS Appl. Mater. Interfaces*, 2016, **8**, 26712–26721.